A Front-Tracking Method for Three-Phase Computations of Solidification with Volume Change

Truong V. Vu[1], Gretar Tryggvason[2], Shunji Homma[3], John C. Wells[1] and Hideyuki Takakura[1]

[1] *Ritsumeikan University, 1-1-1 Nojihigashi, Kusatsu-shi, Shiga 525-8577, Japan*
[2] *Department of Aerospace and Mechanical Engineering, The University of Notre Dame, Notre Dame, IN 46556-5684, USA*
[3] *Division of Materials Science, Saitama University, 255 Shimo-Okubo, Sakura-ku, Saitama-shi, Saitama 338-8570, Japan*

Keywords: Front-Tracking, Solidification, Volume Change, Triple Point, Drop

We use a front-tracking method to simulate solidification with volume change of a droplet on a fixed cooling plate. The problem includes temporal evolution of three interfaces, i.e., solid–liquid, solid–air, and liquid–air, that are explicitly tracked under the assumption of axisymmetry. The solid–liquid interface is propagated with a normal velocity that is calculated from the normal temperature gradient across the front and the latent heat. The liquid–air front is advected by the velocity interpolated from nearest bulk fluid flow velocities. Accordingly, the evolution of the solid–air front is simply the temporal imprint of the triple point at which simple and straightforward conditions are imposed. The governing Navier–Stokes equations are solved for the whole domain, setting the velocities in the solid phase to zero and with the non-slip condition on the solid–liquid interface. Computational results are compared with exact solutions for two-dimensional Stefan problems and with corresponding experimental results, and show good agreement.

Introduction

A solidification problem in which there is the presence of solid, liquid and gas appears in many methods of growing crystals from melts such as Czochralski crystal growth (Porrini, 2001), float-zone processing (Markvart, 2000), laser welding (Booth, 2004) and spraying (Minemoto and Takakura, 2007). The three phases meet at the tri-junction, and the solid phase comes directly from the melt. The evolution of the solidification interface, i.e., the interface separating solid and liquid, and the tri-junction conditions determine the form of the solidified product. In addition, density difference between solid and liquid in conjunction with the tri-junction effect can produce a curious shape (Ajaev and Davis, 2004).

Recently, a drop solidifying on a cold plate, which includes the above-mentioned aspects, has been paid much attention to. Experimental studies can be found in Anderson *et al.* (1996), Satunkin (2003) and Hu *et al.* (2010). However, direct numerical simulations of this problem are still lacking. Schultz *et al.* (2001) used a boundary integral method to investigate a drop solidifying on a cold plate (Anderson *et al.*, 1996), but neglecting the gravity effect. A similar method with fixed contact angles has been used by Ajaev and Davis (2004) to consider the effect of the density difference and contact angles on the shape of the solidified drop under zero gravity. Virozub *et al.* (2008) included the gravity and surface tension effects to the problem. The Young–Laplace equation in conjunction with a constant growth angle was numerically solved to find the position of the liquid–gas front. In another work (Pasandideh-Fard *et al.*, 2002), the volume of fluid combined with the enthalpy method has been used to investigate the solidification process of a drop. However, volume change was not accounted for.

In this paper, we deal with the solidification process, which includes volume change and the tri-junction and gravity effects. We base on the front-tracking/finite difference method for dendritic solidification (Al-Rawahi and Tryggvason, 2002) and impose simple and straightforward tri-junction conditions to simulate a drop solidifying on a cold plate.

1. Mathematical Formulation and Numerical Method

Figure 1(a) shows the investigated problem. An axisymmetric drop contacts with a cold plate at cold temperature T_c and then solidifies from the bottom. Initially, the liquid drop surrounded by ambient (gas) at temperature T_g is at hot temperature T_h that is greater than or equal to its melting temperature T_m. During solidification, the volume change and the tri-junction play an important role in the ultimate shape of the drop. In addition, in the case of water, there exists evaporation from the freezing drop, which generates a condensation halo around the drop (Jung *et al.*, 2012). Formation of evaporation and halos also affects the solidification process. However, in this paper we neglect the effect of

Received on July 18, 2013; accepted on September 7, 2013
DOI: 10.1252/jcej.13we169
Correspondence concerning this article should be addressed to T. V. Vu (E-mail address: vvt_gago@yahoo.com).

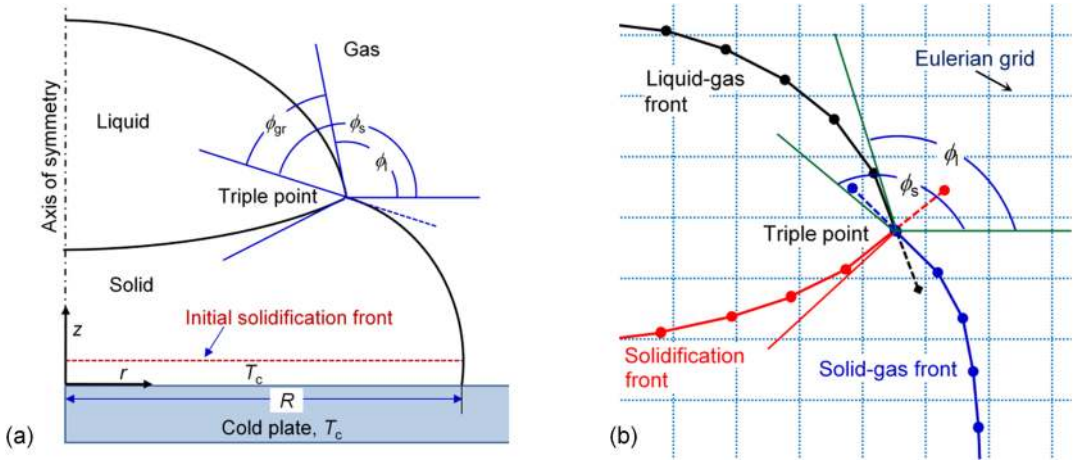

Fig. 1 A drop solidifying on a cold plate: (a) computational domain and (b) triple point treatment. In (b), solid elements represent actual fronts and dash elements are extended ones to account for calculations of contact angles and surface tension force

the evaporation and condensation halo. The focus points are volume change caused by density difference between solid and liquid, and effect of the tri-junction.

Here, we assume that the fluids are incompressible, immiscible and Newtonian. We treat all phases as one fluid with variable properties such as density ρ, viscosity μ, thermal conductivity k and heat capacity C_p. Accordingly, the governing equations are given as Eqs. (1) to (3). The heat source at the solidification front $\dot{q}_f$ is given as Eq. (4).

$$\frac{\partial(\rho\mathbf{u})}{\partial t}+\nabla\cdot\rho\mathbf{u}\mathbf{u}=-\nabla p+\nabla\cdot[\mu(\nabla\mathbf{u}+\nabla\mathbf{u}^T)]+\rho\mathbf{g}+\int_f\sigma\kappa\delta(\mathbf{x}-\mathbf{x}_f)\mathbf{n}_f\mathrm{d}S \quad (1)$$

$$\frac{\partial}{\partial t}(\rho C_pT)+\nabla\cdot(\rho C_pT\mathbf{u})=\nabla\cdot(k\nabla T)+\int_f\dot{q}_f\delta(\mathbf{x}-\mathbf{x}_f)\mathrm{d}S \quad (2)$$

$$\nabla\cdot\mathbf{u}=(1/\rho_s-1/\rho_l)\int_f\delta(\mathbf{x}-\mathbf{x}_f)\dot{q}_f\mathrm{d}S\Big/L_h \quad (3)$$

$$\dot{q}_f=k_s\frac{\partial T}{\partial n}\bigg|_s-k_l\frac{\partial T}{\partial n}\bigg|_l \quad (4)$$

Equation (3) accounts for volume change at the solidification front due to density difference between solid and liquid.

We use here a front-tracking/finite difference method (Esmaeeli and Tryggvason, 2004) with modification to account for the presence of three phases, phase change and volume change. The three phases and their properties are specified using indicator functions that are determined from known positions of the interface points: the points of the solidification and solid–gas fronts are used to construct the indicator I_s ($I_s=0$ in solid and $I_s=1$ in liquid and gas) while the indicator I_l ($I_l=0$ in liquid and solid and $I_l=1$ in gas) is built from the points on the solid–gas and liquid–gas interfaces. Accordingly, the values of the material property fields at every location are then given by

$$\phi=\phi_gI_l+(1-I_l)[\phi_lI_s+(1-I_s)\phi_s] \quad (5)$$

Here, ϕ stands for ρ, μ, C_p, or k. I_s is also used to set velocity field in the solid phase to zero. A detailed description of how to solve the above governing equations can be found in Esmaeeli and Tryggvason (2004). Here we just describe how to incorporate conditions at the tri-junction, i.e., triple point in 2D view as shown in **Figure 1(b)**. We have three types of interfaces represented by connected elements that move on a stationary grid. The solidification front propagates with the normal velocity V_n, $V_n=\dot{q}_f/(\rho_sL_h)$ while the liquid–gas front is advected by the velocity interpolated from the fixed grid velocities. At the triple point, we correct the position of this point by applying a constant growth angle (Virozub *et al.*, 2008). We do this by introducing an extended element at the end of each interface. We then estimate the tangent vector of each interface at the triple point by fitting a third-order polynomial through the triple point, the other point on the extended element and two adjacent points on the nearest elements. Thereby, the growth angle is defined as $\phi_{gr}=\theta_s-\theta_l$ where θ_s and θ_l are the angles between the tangent to the solid–air interface and the horizontal and between the tangent to the liquid–air interface and the horizontal. We adjust the position of the triple point to satisfy the prescribed growth angle using the secant method.

2. Numerical Parameters

We choose the wetting radius R as a scaling length, and $\tau_c=\rho_lC_lR^2/k_l$ as the characteristic time scale. The characteristic velocity scale is thus not independent and is taken to be $U_c=R/\tau$. With these above choices, it is possible to show that the dynamics of the problem is governed by the following dimensionless parameters: Prandtl number $Pr=C_p\mu_l/k_l$; Stefan number $St=(T_m-T_c)/L_h$; Bond number $Bo=\rho_lgR^2/\sigma$; Weber number $We=\rho_lU_c^2R/\sigma$; density ratios $\rho_{sl}=\rho_s/\rho_l$ and $\rho_{gl}=\rho_g/\rho_l$ viscosity ratios $\mu_{sl}=\mu_s/\mu_l$ and $\mu_{gl}=\mu_g/\mu_l$; thermal conductivity ratios $k_{sl}=k_s/k_l$ and $k_{gl}=k_g/k_l$; heat capacity ratios $C_{psl}=C_{ps}/C_{pl}$ and $C_{pgl}=C_{pg}/C_{pl}$. The temperature is nondimensionalized as $\Theta=(T-T_c)/(T_h-T_c)$. The non-dimensional time is $\tau=t/\tau_c$.

Most of the experimental studies mentioned previously

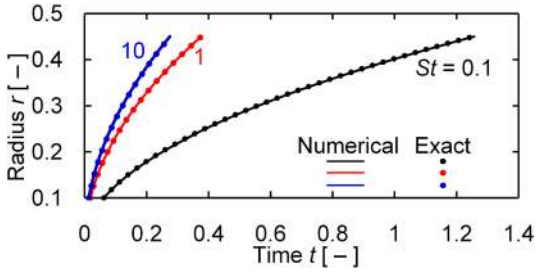

Fig. 2 Comparisons with exact solutions of Carslaw and Jaeger (1986)

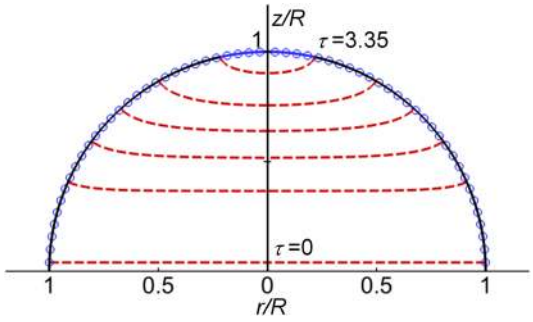

Fig. 3 Method verification: dash and solid lines represent solidification and solid–gas fronts; circles represent the initial liquid–gas front. The solidification front is plotted every $\Delta\tau = 0.67$

concern the solid–liquid–gas systems. The density and viscosity ratios of liquids to gas are very high. However, our simulation results presented in this paper are limited to cases of moderate ratios of viscosity and density since, at high density ratios with high interfacial tension, typical of liquid–gas systems, high and irregular velocities appearing near the interfaces destroy the solution (Tryggvason *et al.*, 2011). In addition, high density and viscosity ratios result in a high computational cost. However, as shown below, our approximations for the density and viscosity ratios as well as for ratios of thermal properties are reasonable.

3. Results and Comparisons

We first compare our computational results with analytical solutions for a 2D Stefan problem (Carslaw and Jaeger, 1986) in which a line heat source Q causes a circular solid seed at the center to evolve in the direction of increasing the radius of the seed. Simulations are performed for this 2D problem set at $St = C_{ps}/(k_s L_h) = 0.1$, 1, and 10. The initial front location and temperature used for simulations are found from the exact solutions at the moment $t = t_0$ when a small, circular solid seed with a radius $r = 0.1$ has formed. Q is set at 10. **Figure 2** shows that the computational results agree well with the exact solutions at different Stefan numbers.

To verify the method, we investigate a case of drop solidification with $Pr = 0.02$, $St = 0.1$, $Bo = 0$, $We = 1$, $k_{sl} = 1$, $k_{gl} = 0.01$, $C_{psl} = C_{pgl} = 1$, $\mu_{sl} = 5$, $\mu_{gl} = 0.1$, $\rho_{sl} = 1$, $\rho_{gl} = 0.1$ and $\phi_{gr} = 0°$. Since there is no volume change with a zero growth angle, the shape of the solidified drop must be the same as that of the initial liquid drop (Ajaev and Davis, 2004). **Figure 3** confirms this.

Next, we turn to the cases in which there exists volume change in conjunction with constant growth angles. In all cases presented below, at the beginning of computation $\tau = 0$, a thin solid layer at $\Theta = 0$ has formed at the cold plate, as shown in Figures 5 to 7.

Figure 4 shows the solidification process of a water drop on a cold plate (Hu *et al.*, 2010) with $Pr = 7.25$, $St = 0.025$, $Bo = 0.025$, $We = 5\times10^{-5}$, $k_{sl} = 3.8$, $k_{gl} = 0.04$, $C_{psl} = 0.5$, $C_{pgl} = 0.24$, $\mu_{sl} = 5$, $\mu_{gl} = 0.05$, $\rho_{sl} = 0.9$, $\rho_{gl} = 0.05$, and $\phi_{gr} = 0°$. The liquid drop initially has a spherical cap. During the freezing process, heat in the liquid phase is released to the gas and solid phase, leading to a decrease in the temperature. The velocity field (on the right of Figure 4) indicates

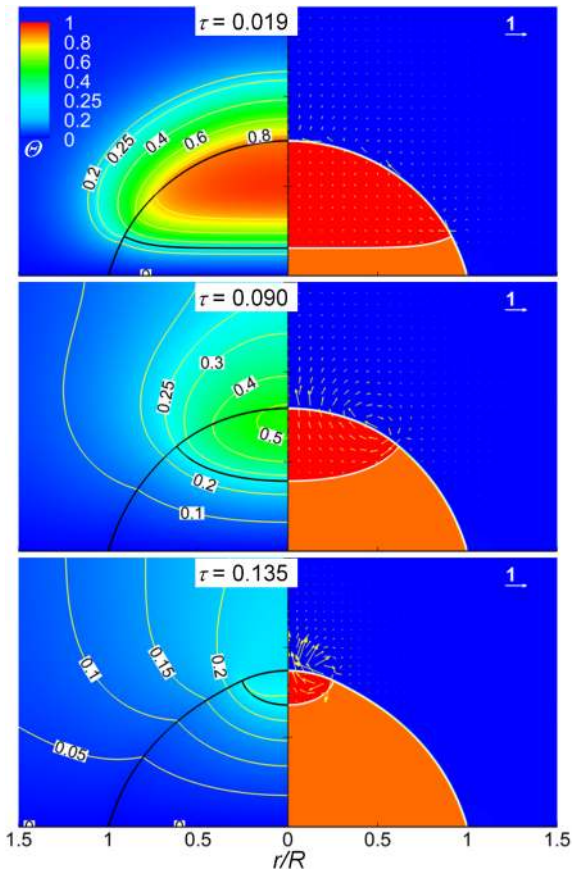

Fig. 4 Solidification process of a water drop: The left showing the temperature field and the right showing the velocity field normalized by U_c. Yellow lines on the left represent the temperature contours

that the drop tends to expand in the vertical direction rather than in the horizontal direction (Enríquez *et al.*, 2012). In addition, the velocity field becomes stronger as the liquid part decreases. This causes heat in the liquid phase to be transferred faster to the gas phase during the last stages of solidification. Detailed evolution of the solidification front is shown in **Figure 5(a)** with a comparison with the experimental drop shape reported in Hu *et al.* (2010) (**Figure 5(b)**). Because of different density of the solid and liquid phases, the shape of the solidified drop is profoundly differ-

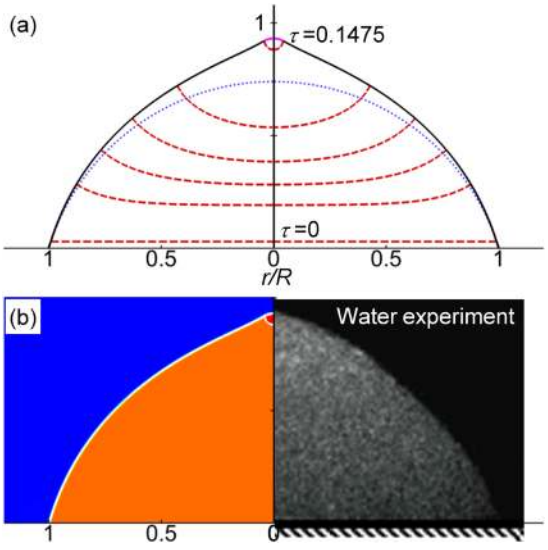

Fig. 5 Solidification of a water drop: (a) Evolution of the solidification front (dash line plotted every $\Delta\tau=0.0295$); and (b) a comparison with the experimental solidified drop shape reported in Hu *et al.* (2010). In (a), the dot line represents the initial liquid–gas front

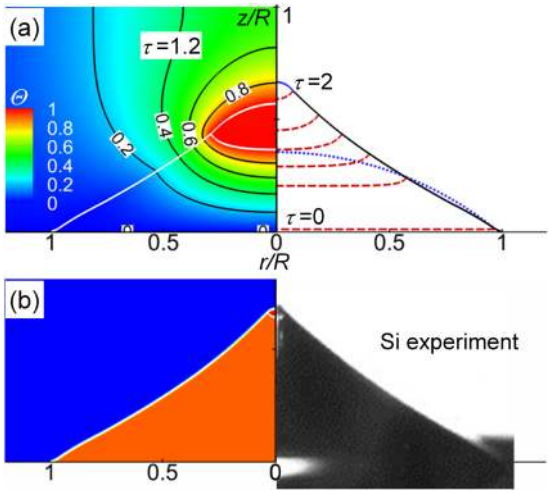

Fig. 6 Solidification of a Si drop. (a) The left shows the temperature contours at $\tau=1.2$, and the right shows evolution of the solidification front (dash line plotted every $\Delta\tau=0.4$). (b) A comparison with the experimental solidified drop shape reported in Satunkin (2003). In (a), the dot line on the right represents the initial liquid–gas front

ent from the liquid one. Figure 5(a) also indicates that the growth rate is high during the initial stages of solidification because of a large temperature gradient. When the solidification front goes further, the solidification rate gradually decreases (Ajaev and Davis, 2004). However, when the drop has nearly solidified, the growth rate again increases since the interface area shrinks to zero (Schultz *et al.*, 2001). The comparison with the experimental solidified drop shape shows good agreement.

Figure 6(a) shows the solidification process of a drop with $Pr=0.013$, $St=0.116$, $Bo=1.32$, $We=0.05$, $k_{sl}=0.5$, $k_{gl}=0.01$, $C_{psl}=C_{pgl}=1$, $\mu_{sl}=5$, $\mu_{gl}=0.05$, $\rho_{sl}=0.91$, and $\rho_{gl}=0.05$. These parameters except for *We* correspond to silicon (Si) (Satunkin, 2003). The growth angle ϕ_{gr} is set to 12° according to the experiment of Satunkin (2003). Initially, the liquid–gas interface is spherical, and the liquid phase is at $T_h=T_m$. During solidification, the temperature in the liquid phase keeps at the melting temperature. Good agreement between computational and experimental solidified drop shape has been found as shown in **Figure 6(b)**.

Figure 7(a) shows the solidification process of a drop with $Pr=0.0255$, $St=0.278$, $Bo=0.6$, $We=0.008$, $k_{sl}=0.39$, $k_{gl}=0.01$, $C_{psl}=0.77$, $C_{pgl}=3.7$, $\mu_{sl}=5$, $\mu_{gl}=0.03$, $\rho_{sl}=0.8$, and $\rho_{gl}=0.05$. These parameters except for *We* correspond to indium antimonide (InSb) (Satunkin, 2003). Initially, the liquid phase has a spherical cap. Satunkin (2003) reported that the growth angle increases, in the range of 25 to 30°, with a decrease in the wetting radius. And this variable growth angle could be easily taken into account in our codes. However, ϕ_{gr} here is fixed at 25°, and reasonable agreement between the computational and experimental solidified drop shape is found as shown in **Figure 7(b)**.

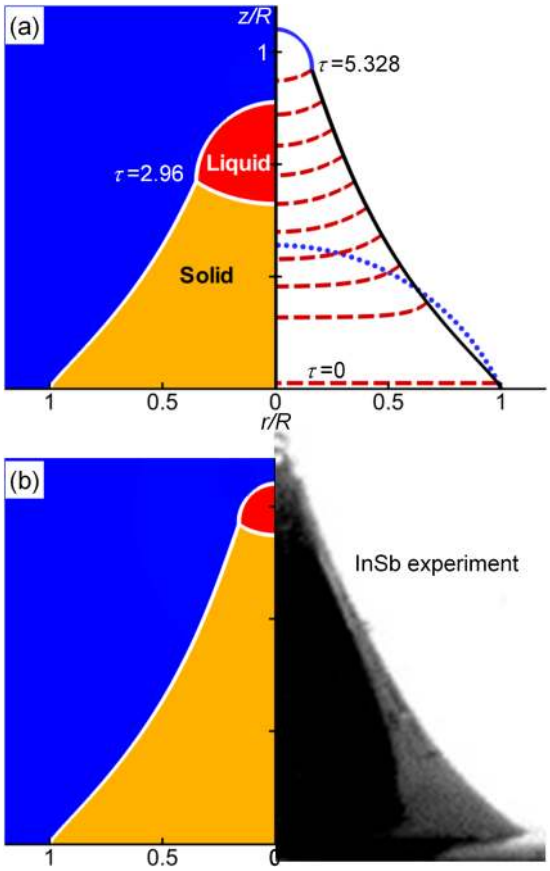

Fig. 7 Solidification of an InSb drop. (a) The left shows the drop states at $\tau=2.96$ and the right shows evolution of the solidification front (dash plotted every $\Delta\tau=0.592$). (b) A comparison with the experimental solidified drop shape reported in Satunkin (2003). In (a), the dot line on the right represents the initial liquid–gas front

4. Discussion

During the solidification, the liquid phase is confined by balance of the interfacial tension and the gravitational forces, while the volume change and the solidified drop shape are mainly caused by both the difference between density of solid and liquid and the growth angle. In the case of zero growth angle, e.g. Figures 4 and 5, a cone formed near the axis of symmetry is mainly due to the density ratio (Anderson *et al.*, 1996). Figures 5 and 7 show that the increasing the solid–liquid density ratio increases the corner angle at the top of the solidified drop (Ajaev and Davis, 2004). This angle also increases as the growth angle decreases, see Figures 5–7.

The main focus in this paper is to demonstrate the capability of the front-tracking method for the problems including the volume change and the tri-junction effect. We just reproduced, with some assumptions, the solidified drop shape observed in the related experiments. Even though good agreement has been found, there have been still many unresolved issues. For instance, how the non-dimensional parameters affect the solidified drop shape as well as the solidification rate. In addition, more physics such as Marangoni effect, evaporation and formation of the condensation halo should be added to the method to provide more accurate solutions.

Conclusions

We have presented a front-tracking method for simulation of the drop solidification with volume change. The solidification and liquid–gas interfaces are updated in different ways while the evolution of the solid–gas interface is determined by the triple point conditions. At this point we applied a constant growth angle. The computational method was applied to simulate the solidification process of water, Si and InSb drops. After solidification, a cusp forms near the axis of symmetry. Comparisons with corresponding experiments show that the method yielded the reasonably accurate solidified drop shape.

Acknowledgements

The first author would like to thank JSPS (Japan Society for the Promotion of Science) for their financial supports during his study at Ritsumeikan University (Japan). This work was partially supported by JSPS KAKENHI Grant Number 24–384.

Nomenclature

C_p	=	specific heat capacity	[J/(kg K)]
$\mathbf{g}$	=	gravitational acceleration	[m/s^2]
I	=	indicator function	[—]
k	=	thermal conductivity	[W/(m K)]
L_h	=	latent heat of fusion	[J/kg]
$\mathbf{n}$	=	unit normal vector	[—]
p	=	pressure	[N/m^2]
q	=	heat flux	[W/m^2]
R	=	wetting radius	[m]
S	=	surface	[m^2]
T	=	temperature	[K]
t	=	time	[s]
U_c	=	characteristic velocity	[m/s]
$\mathbf{u}$	=	velocity vector	[m/s]
V_n	=	solidification rate	[m/s]
$\mathbf{x}$	=	position vector	[m]
δ	=	delta function	[m^{-3}]
ϕ_{gr}	=	growth angle	[°]
κ	=	curvature	[m^{-1}]
μ	=	viscosity	[Pa s]
θ	=	contact angle	[°]
ρ	=	density	[kg/m^{-3}]
σ	=	interfacial coefficient	[N/m]
τ	=	dimensionless time	[—]
Θ	=	dimensionless temperature	[—]

‹Subscripts›

c	=	cold
f	=	interface
g	=	gas, air
h	=	hot
l	=	liquid
m	=	melting
s	=	solid
T	=	transpose

Literature Cited

Ajaev, V. S. and S. H. Davis; "The Effect of Tri-Junction Conditions in Droplet Solidification," *J. Cryst. Growth*, **264**, 452–462 (2004)

Al-Rawahi, N. and G. Tryggvason; "Numerical Simulation of Dendritic Solidification with Convection: Two-Dimensional Geometry," *J. Comput. Phys.*, **180**, 471–496 (2002)

Anderson, D. M., M. G. Worster and S. H. Davis; "The Case for a Dynamic Contact Angle in Containerless Solidification," *J. Cryst. Growth*, **163**, 329–338 (1996)

Booth, H. J.; "Recent Applications of Pulsed Lasers in Advanced Materials Processing," *Thin Solid Films*, **453–454**, 450–457 (2004)

Carslaw, H. S. and J. C. Jaeger; Conduction of Heat in Solids, 2nd ed., Oxford University Press, New York, U.S.A. (1986)

Enríquez, O. R., Á. G. Marín, K. G. Winkels and J. H. Snoeijer; "Freezing Singularities in Water Drops," *Phys. Fluids*, **24**, 091102, 091102–2 (2012)

Esmaeeli, A. and G. Tryggvason; "A Front Tracking Method for Computations of Boiling in Complex Geometries," *Int. J. Multiphase Flow*, **30**, 1037–1050 (2004)

Hu, H., Z. Jin, D. Nocera, C. Lum and M. Koochesfahani; "Experimental Investigations of Micro-Scale Flow and Heat Transfer Phenomena by Using Molecular Tagging Techniques," *Meas. Sci. Technol.*, **21**, 085401 (2010)

Jung, S., M. K. Tiwari and D. Poulikakos; "Frost Halos from Supercooled Water Droplets," *Proc. Natl. Acad. Sci. USA*, **109**, 16073–16078 (2012)

Markvart, T.; Solar Electricity, 2nd ed., Wiley, New York, U.S.A. (2000)

Minemoto, T. and H. Takakura; "Fabrication of Spherical Silicon Crystals by Dropping Method and Their Application to Solar Cells," *Jpn. J. Appl. Phys.*, **46**(7A), 4016–4020 (2007)

Pasandideh-Fard, M., S. Chandra and J. Mostaghimi; "A Three-Dimensional Model of Droplet Impact and Solidification," *Int. J. Heat Mass Transfer*, **45**, 2229–2242 (2002)

Porrini, M.; "Czochralski Silicon," Encyclopedia of Materials: Science and Technology, 2nd ed., pp. 1965–1970, Elsevier, Oxford, U.K. (2001)

Satunkin, G. A.; "Determination of Growth Angles, Wetting Angles, Interfacial Tensions and Capillary Constant Values of Melts," *J. Cryst. Growth*, **255**, 170–189 (2003)

Schultz, W. W., M. G. Worster and D. M. Anderson; "Solidifying Sessile Water Droplets," Interactive Dynamics of Convection and Solidification, pp. 209–226, Kluwer Academic Publishers, Dordrecht, the Netherlands (2001)

Tryggvason, G., R. Scardovelli and S. Zaleski; Direct Numerical Simulations of Gas–Liquid Multiphase Flows, Cambridge University Press, Cambridge, U.K. (2011)

Virozub, A., I. G. Rasin and S. Brandon; "Revisiting the Constant Growth Angle: Estimation and Verification via Rigorous Thermal Modeling," *J. Cryst. Growth*, **310**, 5416–5422 (2008)